

Spin-liquid properties of a capped kagome molecule with 60 magnetic centers

Roman Rausch¹, Matthias Peschke^{2,3}, Cassian Plorin^{3,4}, Christoph Karrasch¹

1 Technische Universität Braunschweig, Institut für Mathematische Physik,
Mendelssohnstraße 3, 38106 Braunschweig, Germany

2 Institute for Theoretical Physics Amsterdam and Delta Institute for Theoretical
Physics, University of Amsterdam, Science Park 904, 1098 XH Amsterdam, The
Netherlands

3 I. Institute of Theoretical Physics, University of Hamburg, Notkestraße 9, 22607
Hamburg, Germany

4 The Hamburg Centre for Ultrafast Imaging, Luruper Chaussee 149, 22761 Hamburg,
Germany

* r.rausch@tu-braunschweig.de

November 8, 2021

1 Abstract

2 We compute ground-state properties of the isotropic, antiferromagnetic Heisenberg model
3 on the sodalite cage geometry. This is a 60-spin spherical molecule with 24 vertex-sharing
4 tetrahedra which can be regarded as a molecular analogue of a capped kagome lattice
5 and which has been synthesized with high-spin rare-earth atoms. Here, we focus on the
6 $S = 1/2$ case, where spin-liquid effects are expected. We employ the SU(2)-symmetric
7 density-matrix renormalization group (DMRG), which is a highly accurate numerical tool.

8 We find a threefold degenerate ground state that breaks the spatial symmetry and that
9 splits up the molecule into three large parts which are almost decoupled from each other.
10 This can be regarded as a generalization of a valence-bond-solid state (VBS) and is in stark
11 contrast to the behaviour of most known spherical molecules. On a methodological level,
12 the disconnection leads to “glassy dynamics” within the DMRG that cannot be targeted
13 via standard techniques.

14 In the presence of finite magnetic fields, we find broad magnetization plateaus at
15 “magic values” of $4/5$, $3/5$, and $1/5$ of the saturation, which one can understand in terms
16 of localized magnons, singlets, and doublets which are again nearly decoupled from each
17 other. The plateaus should be observable experimentally and might serve as a signature
18 to validate the use of the $S = 1/2$ Heisenberg model for a given system. At the saturation
19 field, the zero-point entropy is $S = \ln(181) \approx 5.2$ in units of the Boltzmann constant.

20

21 Contents

22	1 Introduction	2
23	2 Geometry	4
24	3 Technical details	5
25	4 Symmetry-broken ground state	5

26	5	Nearly disconnected subsystems	8
27	6	Finite magnetic fields	9
28	6.1	Localized magnons	9
29	6.2	Localized singlets and doublets	12
30	7	Conclusion	13
31	A	Symmetry transformations for the SOD60 molecule	14
32		References	16

33
34

35 1 Introduction

36 Interacting quantum spins have a tendency to form singlet states, which have no preferred
37 direction and minimize the antiferromagnetic exchange energy. This is captured by the
38 Heisenberg Hamiltonian

$$H = \sum_{ij} J_{ij} \mathbf{S}_i \cdot \mathbf{S}_j, \quad (1)$$

39 where J_{ij} are the exchange couplings among L spins, and $\mathbf{S}_i = (S_i^x, S_i^y, S_i^z)$ is a vector
40 of spin- S operators. This singlet formation is frustrated on non-bipartite lattices, among
41 which vertex-sharing triangular geometries (kagome-type) and vertex-sharing tetrahedral
42 geometries (pyrochlore-type) stand out as particularly complicated and interesting. Such
43 systems can be roughly grouped into (i) 1D chains, (ii) 2D/3D lattices, and (iii) finite
44 molecules. Among the molecules, ferric wheels are analogous to 1D chains or ladders [1, 2],
45 while hollow cages [3–10] (such as the Platonic or Archimedean solids) are analogous to
46 2D planes, albeit with a spherical topology.

47 In this work, we focus on the physics of quantum spins in molecular systems. One
48 of the most well-studied molecules is the icosidodecahedron, a molecular analogue of the
49 kagome lattice [3, 5–9]. This 30-site spherical cage can be formed by transition metal
50 ions V^{4+} , Cr^{3+} , Fe^{3+} in the Keplerate molecules [11–13] with $S = 1/2$, $3/2$, and $5/2$,
51 respectively. Recently, a cage-like molecule with $L = 60$ spins was synthesized that is
52 based on vertex-sharing tetrahedra [14] and that can be classified as a molecular analogue
53 of a capped kagome compound [15–17] (see Fig. 1). The addition of the “caps” promotes
54 the triangles to tetrahedra and is a step towards the 3D pyrochlore lattice.

55 Due to the high frustration and three-dimensionality of the pyrochlore lattice, not
56 much is known about the ground state of the isotropic Heisenberg model on this geometry.
57 Neither the value of the ground state energy nor the existence of a spin gap have been
58 reliably estimated [18, 19] despite a wealth of approaches. Exact diagonalization reaches its
59 limits with about 36 sites [20, 21] and finds a disordered spin-liquid ground state. On the
60 other hand, approximate results (often based on weakening the intertetrahedra coupling J'
61 to obtain a small expansion parameter) see lattice symmetry breaking [22–26]. However,
62 such methods may not properly take into account the competition between different phases.
63 Recent progress involves the application of the pseudofermion functional renormalization
64 group [18], where such competition is thought to be treated more faithfully and which
65 again points to a spin-liquid ground state. An approach coming from the high-temperature
66 region comparing various imaginary-time propagation techniques [19] indicates that much

67 of the entropy is unreleased before low temperatures can be reached, pointing towards
 68 a high density of states close to $T = 0$. One should note that in contrast to the 3D
 69 pyrochlore lattice, a 60-spin molecule can be treated accurately using the density-matrix
 70 renormalization group (DMRG), while still having a non-trivially large size.

71 In experimental realizations of the capped kagome molecule [14], the spin centres are
 72 Gd atoms with $S = 7/2$ (Dy, Er and Y were also used [27, 28]). This allows for an
 73 approximation with classical spins, and it was shown that the system can be described well
 74 by the classical isotropic Heisenberg model [14]. While the absence of a strong anisotropy
 75 prevents Ising-like ordering and is a prerequisite to observe spin-liquid effects, such effects
 76 are washed out by the large value of S . This motivates us to look at the same geometry
 77 for the case of $S = 1/2$, where quantum fluctuations are the strongest.

78 There are several scenarios for the nature of the ground state of such a frustrated spin
 79 system. One possibility is an ordered state which breaks the spin symmetry and which is
 80 found, e.g., for the triangular lattice [29–32]. Another possibility is a “valence-bond solid”
 81 (VBS) in which translational invariance is broken by a particular pair-singlet covering.
 82 However, spin symmetry remains unbroken, so that the total spin S_{tot} obtained from

$$\langle \mathbf{S}_{\text{tot}}^2 \rangle = \sum_{ij} \langle \mathbf{S}_i \cdot \mathbf{S}_j \rangle = S_{\text{tot}} (S_{\text{tot}} + 1) \quad (2)$$

83 is zero. A VBS state tends to appear for fine-tuned parameters or very small sys-
 84 tems [33–36]. Yet another possibility is that the ground state is highly degenerate due
 85 to the exponentially large number of combinations to distribute pair-singlets in 2D and
 86 3D [37]. However, this degeneracy tends to split into a unique “liquid” ground state
 87 with exponentially decreasing correlations and many low-lying singlet states. The latter
 88 case is what is found for frustrated polyhedra, such as the icosahedron ($L = 12$) [4], the
 89 cuboctahedron ($L = 12$) [5, 6], the dodecahedron ($L = 20$) [4], and the icosidodecahedron
 90 ($L = 30$) [3, 5–9]. They have nondegenerate ground states that transform according to the
 91 trivial irreducible representation A_{1g} of the icosahedral group I_h or the octahedral group
 92 O_h , as well as a number of low-lying $S_{\text{tot}} = 0$ states that grows quickly with the size.

93 In this paper, we will show that unlike these smaller polyhedra the ground state of our
 94 large capped-kagome molecule is not given by the trivial irreducible representation A , but
 95 rather by T , making it threefold degenerate and thus in principle symmetry-broken. Each
 96 member of the ground-state manifold can be conceptualized as follows: The two poles
 97 and a belt around the equator of the sphere nearly completely decouple from each other
 98 and the rotational symmetry is reduced to rotations about only one coordinate axis. The
 99 different ground states are thus related by a global reshuffling of the spins of the whole
 100 molecule which cannot be achieved with local operations in reasonable time and which
 101 leads to a “glassy” behaviour for the DMRG algorithm (which hinges on local updates).
 102 To the best of our knowledge, such a state has not been found elsewhere and is thus a new
 103 addition to the list of possible scenarios for the ground states of frustrated geometries.

104 After computing the ground state, we analyze the behavior of several physical quanti-
 105 ties. We demonstrate the existence of localized magnons, resulting in a zero-point entropy
 106 of $S = \ln(181) k_B \approx 5.2 k_B$ per molecule (k_B : Boltzmann constant) at the saturation
 107 magnetization. We observe wide magnetization plateaus at $3/5$ and $1/5$ of the saturation,
 108 which can be explained by commensurate numbers of spinflips that can form localized con-
 109 fined singlet or doublet states. This can be seen as a generalization of localized magnons.

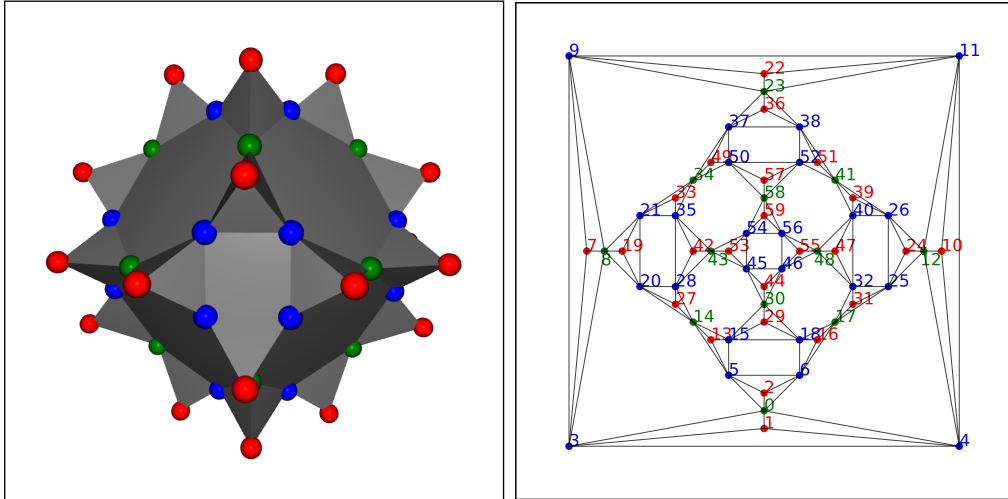


Figure 1: Left: Ball-and-stick drawing of the SOD60 molecule. Right: Projection on the plane (Schlegel diagram) using the square orientation. The enumeration of the sites is the result of applying the Cuthill-McKee compression. Equivalent sites are drawn in the same colour.

110 2 Geometry

111 In a recent work, various hollow cages with magnetic centres have been synthesized, the
 112 largest of which has $L = 60$ spin sites [14]. This cage can be understood by starting
 113 with a *rectified truncated octahedron* [38]. The truncated octahedron is a well-known
 114 Archimedean solid, while the *rectification* procedure is a “shaving off” of the vertices of a
 115 polytope, such that the stubs share a vertex. In this case, it results in 8 hexagon faces, 6
 116 square faces and 24 vertex-sharing triangle faces. Furthermore, each of the 24 triangles is
 117 “capped” (or “stellated”) with an additional spin site, forming vertex-shared tetrahedra.
 118 Thus there are 36 “base spins” residing on the vertices of the polytope and 24 “apex spins”
 119 on top of the triangles. In a different chemical context, this object is known as a “sodalite
 120 cage” [28, 39], commonly abbreviated as SOD. We thus use the shorthand “SOD60” to
 121 refer to this molecule. The geometry is depicted in Fig. 1.

122 There are three inequivalent sites which we depict as red, green, and blue balls in
 123 Fig. 1: (r) the apices of the tetrahedra, (g) the vertices bounded by two hexagons and two
 124 base triangles, (b) the vertices bounded by a hexagon, a square and two base triangles.

125 One finds that there are four inequivalent nearest-neighbour bonds, corresponding
 126 to the connections (r)-(g), (r)-(b), (g)-(b) and (b)-(b). We note that the triangles are
 127 isosceles, with the long edges exceeding the short ones by a factor of $\sqrt{6}/2 \approx 1.22$. One
 128 can therefore expect that this leads to slightly different exchange constants J , but as a
 129 first approach, we assume a homogenous value of $J \equiv 1$ for all nearest neighbours of
 130 the interaction graph J_{ij} . The symmetry group of the molecule is O_h (octahedral) and
 131 has the irreducible representations A (1), E (2), T (3), where the brackets indicate the
 132 multiplicity. The maximal distance of the spin-spin correlations is $d = 7$ and there are 144
 133 nearest-neighbour bonds.

134 We also introduce a new hypothetical cage “SOD20”¹, where the capping procedure
 135 is extended to the triangles of the cuboctahedron, resulting in 12 base spins and 8 apex
 136 spins (see Fig. 4). This leads to a system with $L = 20$ spins, which can be readily solved in

¹We note that SOD20 is distinct from the Gd_{20} system of Ref. 14, which is just a dodecahedron.

137 the full Hilbert space by the Lanczos algorithm, while having a similar geometry and also
 138 belonging to O_h . This is useful as a small system that one can compare to SOD60. We
 139 are not aware of the existence of such a structure, but a cuboctahedron where the squares
 140 are capped instead of the triangles does exist as a Fe-based magnetic molecule [40, 41].

141 3 Technical details

142 In order to find the ground-state wavefunction of the Hamiltonian (1) with $J_{ij} \equiv 1$ for
 143 the bonds depicted in Fig. 1, we employ the DMRG algorithm, which provides a highly
 144 accurate way to variationally determine the ground state within the class of matrix product
 145 states [42]. The dimension of the matrices – the so-called bond dimension – is a measure
 146 of the entanglement and serves as the key numerical control parameter. The reason why
 147 DMRG can tackle exponentially-large Hilbert spaces is that many ground states are only
 148 entangled locally (area law) and can thus be represented faithfully by matrix product
 149 states with a small bond dimension. Our code fully exploits the $SU(2)$ spin symmetry [43]
 150 of the problem. The maximal $SU(2)$ -invariant bond dimension is $\chi_{SU(2)} = 7000$, which
 151 corresponds to an effective bond dimension of about $\chi \sim 30000 - 34000$ when $SU(2)$ is
 152 not exploited. Convergence of the algorithm is assessed by computing the energy variance
 153 per site

$$\Delta E^2/L = \left(\langle H^2 \rangle - \langle H \rangle^2 \right) / L. \quad (3)$$

154 The interaction graph given by J_{ij} is compressed by applying the Cuthill-McKee algo-
 155 rithm [44], which reduces the graph bandwidth to 16. In physical terms, this corresponds
 156 to the maximal hopping distance on the effective 1D chain geometry that is required by
 157 DMRG. The resulting numbering of the sites is displayed in Fig. 1. We refer to Ref. 10 for
 158 a discussion of the dependence of the results on the numbering. We find that the matrix-
 159 product-operator (MPO) representation of the Hamiltonian can be compressed without
 160 losses [45] down to a maximum size of 23×20 .

161 4 Symmetry-broken ground state

162 The left part of Fig. 2 shows the nearest-neighbour spin-spin correlations in the ground
 163 state obtained by DMRG. Evidently, the ground state is symmetry-broken, and instead
 164 of the three rotational axes that pierce the square faces, we are only left with one. This
 165 suggests a threefold degeneracy according to the irreducible representation T . We thus
 166 expect two other ground states to exist that have similarly broken symmetries along the
 167 other two coordinate axes.

168 After computing one member $|E_0\rangle$ of the ground-state manifold, the full multiplet can
 169 be obtained within the DMRG by setting

$$H' = H + E_p |E_0\rangle\langle E_0|, \quad (4)$$

170 where E_p is a sufficiently high energy penalty. The ground state of H' is then a different
 171 member of the multiplet (or the first excited state in case of a non-degenerate ground
 172 state). We find, however, that this technique fails in our case even though we perform
 173 two-site sweeps and apply standard methods of adding fluctuations [42]. The algorithm
 174 always converges to one of many low-lying singlet states whose energy is larger than E_0 .
 175 We will investigate the physical reason for this failure in the next section.

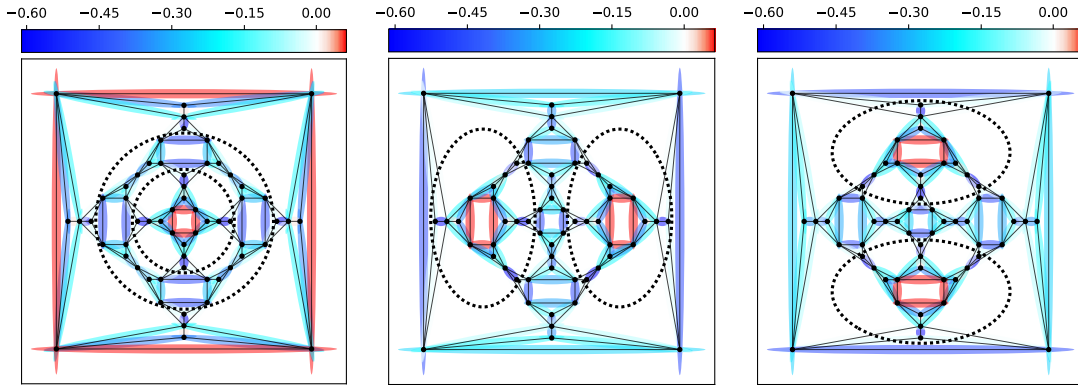


Figure 2: Nearest-neighbour spin-spin correlations $\langle \mathbf{S}_i \cdot \mathbf{S}_j \rangle$ for the three symmetry-broken ground states. The dotted lines indicate where parts of the molecule nearly decouple.

176 To obtain the full multiplet, we need to proceed in a different way. We explicitly
 177 perform a spatial rotation of the state $|E_0\rangle$ such that one ends up with a state that should
 178 correspond to one of the other two members of the ground-state manifold. On a technical
 179 level, this can be achieved by a sequence of transpositions (see App. A for details). For
 180 $S = 1/2$, each transposition is carried out by applying the following operator [46]:

$$P_{12} = 2\mathbf{S}_1 \cdot \mathbf{S}_2 + \frac{1}{2}. \quad (5)$$

181 Acting with P_{12} on an antisymmetric pair-singlet (symmetric pair-triplet) state gives -1
 182 (+1) as an eigenvalue. We find that 45 transpositions are necessary for a rotation by 90
 183 degrees. Such a large product of operators cannot be easily handled in an MPO represen-
 184 tation. The bond dimension increases after each transposition, which makes truncations
 185 necessary and introduces errors. The energy of the rotated state thus becomes significantly
 186 higher than that of the ground state. However, the result can be used as a starting guess
 187 for another DMRG ground state calculation governed by H , which allows us to determine
 188 the ground-state manifold $|E_0^{(a)}\rangle$, $a = 0, 1, 2$, to a satisfactory accuracy. The three ground
 189 states are orthogonal to about $\langle E_0^{(a)} | E_0^{(b)} \rangle = \mathcal{O}(10^{-5})$ ($a \neq b$), and the energy per spin
 190 agrees within four digits (see Fig. 1). The resulting spin-spin correlations are presented
 191 in the central and right part of Fig. 2, where the other two expected symmetry axes are
 192 now apparent. Averaging over the spin-spin correlations

$$\overline{\langle \mathbf{S}_i \cdot \mathbf{S}_j \rangle} = \frac{1}{3} \sum_{a=0}^2 \langle E_0^{(a)} | \mathbf{S}_i \cdot \mathbf{S}_j | E_0^{(a)} \rangle, \quad (6)$$

193 we find that the spatial symmetries are restored, which is shown in Fig. 3. In total, this
 194 provides conclusive evidence for the existence of a symmetry-broken ground state.

195 In principle, one can determine which irreducible representation (T_{1g} , T_{2g} , T_{1u} , or T_{2u})
 196 is associated with the ground-state manifold by computing the corresponding characters.
 197 This requires the evaluation of expectation values $\langle E_0^{(a)} | C | E_0^{(a)} \rangle$, where C represents a
 198 particular rotation or spatial inversion. Since C is either a very large MPO or a product
 199 of many MPOs, such a calculation is not feasible due to the prohibitively large bond
 200 dimension.

a	E	E/L	$\Delta E^2/L$
0	-25.900473	-0.43167	$5.6 \cdot 10^{-5}$
1	-25.895744	-0.43160	$3.6 \cdot 10^{-4}$
2	-25.897953	-0.43163	$2.1 \cdot 10^{-4}$

Table 1: Total energy and energy per spin of the three symmetry-broken ground states, from which $E_0/L = -0.431(7)$ can be estimated. The last column shows the energy variance per site, Eq. (3).

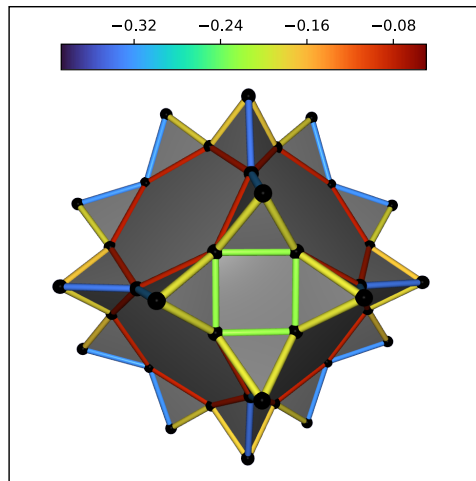


Figure 3: An average of the nearest-neighbour spin-spin correlations across the three ground states via Eq. (6) restores the spatial symmetry.

bond b	$\overline{\langle \mathbf{S} \cdot \mathbf{S} \rangle}_b$
red-green	-0.3241 ± 0.0094
red-blue	-0.1804 ± 0.0060
green-blue	-0.0798 ± 0.0029
blue-blue	-0.2345 ± 0.0073

Table 2: Average of the spin-spin correlations for the inequivalent bonds via Eq. (6). The errors are given by the standard deviation, and the colour labels correspond to the coloured sites in Fig. 1.

201 5 Nearly disconnected subsystems

202 The physical reason behind the failing of the projection technique in Eq. (4) becomes
 203 apparent when examining the spin-spin correlations in Fig. 2 more closely. The dotted
 204 lines intersect the bonds where the correlations are very small, from which one can see
 205 that the molecule breaks up into three nearly decoupled parts, 16 spins on the north and
 206 south pole, respectively, as well as 28 spins on a band along the equator. One way to
 207 quantify this behaviour is to calculate the total spin of the decoupled parts. We find
 208 $\langle \mathbf{S}_{\text{tot}}^2 \rangle \approx 0.15$ for the 16-spin clusters and $\langle \mathbf{S}_{\text{tot}}^2 \rangle \approx 0.3$ on the 28-spin cluster, indicating
 209 that these subsystems are themselves almost singlet states.

210 These observations are reminiscent of a VBS state. However, the decoupled parts are
 211 not just pairs of sites but large subsystems which are positioned at different locations for
 212 each member of the ground-state manifold. Hence, two different members of the ground-
 213 state manifold can only be connected by a global rearrangement of basically all the spins
 214 of the system. It now stands to reason that this is difficult to achieve with local DMRG
 215 updates. Instead, the approach yields local excitations of the disconnected parts. This
 216 is similar to what is usually called “glassy” behaviour: While a state of lower energy
 217 exists, the algorithm is frozen and has trouble finding it with only local updates and with
 218 local interactions. Such behaviour also underlies the anisotropic ferromagnetic Ising model
 219 on the pyrochlore lattice (commonly known as “spin ice”): Theory predicts an extensive
 220 ground-state degeneracy due to the strong frustration, which contradicts the third law of
 221 thermodynamics. One thus expects that a small perturbation will break the degeneracy
 222 and prefer a certain configuration, yet the degeneracy is also measured experimentally. The
 223 reason seems to be that approaching the true ground state requires a large number of spin
 224 flips, which is improbable and does not happen on the experimental timescale [47]. This
 225 leaves the system trapped in various local minima, similar to how the DMRG algorithm
 226 is trapped when trying to solve Eq. (4).

227 We might in fact also compare the situation with intrinsic topological order, which is
 228 found for the toric code model or for quantum dimer models in 2D [47–50]. In such a state,
 229 the ground-state degeneracy depends on the topology of the space the system is confined
 230 to, and each member of the ground-state manifold has a distinct winding number. This
 231 winding number is preserved exactly and cannot be changed by the Hamiltonian. In our
 232 case, the disconnection is only approximate, i.e., connecting the ground states is difficult
 233 in practice by a local Hamiltonian and only with local updates.

234 We point out that a symmetry-broken ground state with two nearly disconnected
 235 parts only appears for a system that is large enough and thus constitutes a many-body
 236 effect. Figure 4 shows the nearest-neighbour spin-spin correlations of the smaller SOD20
 237 molecule, which can be solved using exact diagonalization. We find a unique ground state
 238 with $E_0/L = -0.43440$ with no broken symmetries.

239 Finally, we remark that exactly confined states are also known from the solution of the
 240 tight-binding Hamiltonian on the Penrose lattice [51, 52], which is, however, bipartite.

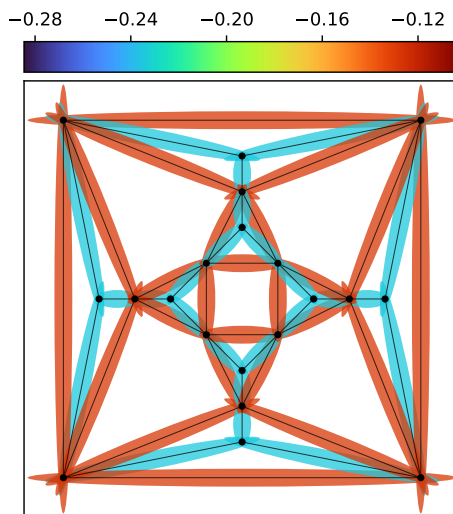


Figure 4: Nearest-neighbour spin-spin correlations of the hypothetical SOD20 molecule (a cuboctahedron where each triangle face is decorated (capped) with an additional apex spin site); only two distinct values appear, -0.2346 for the apex spins and -0.1274 for the base spins, respectively. The ground state is unique with no broken symmetries. The results were obtained using exact diagonalization.

241 6 Finite magnetic fields

242 We now study the properties of SOD60 in the presence of a finite magnetic field B . In
 243 Fig. 6, we show the magnetization $M = S_{\text{tot}}$ as a function of B in the ground state of
 244 SOD60 as well as of the hypothetical SOD20 molecule. The results were obtained by
 245 computing the lowest energy state in each sector of the total spin S_{tot} with an $SU(2)$ -
 246 invariant bond dimension of $\chi_{SU(2)} = 3000$ (which, e.g., corresponds to $\chi \sim 85000$ in the
 247 sector with $S_{\text{tot}} = 18$ if no symmetries are exploited).

248 Most notably, we observe wide magnetization plateaus that appear at “magic frac-
 249 tions” $1/5$, $3/5$, and $4/5$ of the saturation value. Their broadness implies that they are
 250 thermodynamically stable and should be observable in the experiment. Such a signa-
 251 ture could serve as a check that a given system can indeed be described by an isotropic
 252 $S = 1/2$ Heisenberg model. We note that a wide $3/5$ plateau was experimentally observed
 253 in a capped kagome chain with $S = 1/2$ based on Cu [17], though its ground state was
 254 found to have long-ranged canted antiferromagnetic order.²

255 We will now try to understand the reason for the appearance of the wide magnetization
 256 plateaus as well as the nature of the corresponding magic fractions. At large fields, this
 257 can be achieved by using the picture of localized magnons.

258 6.1 Localized magnons

259 The emergence of localized magnons due to frustration is an effect that is described in detail
 260 in various publications [54–59]. Here, we focus on the essential quantitative properties for
 261 the SOD60 molecule. In short, an eigenstate of the system one spinflip away from the

²Theoretically, one expects a width of $0.75 - 7.5$ T if one assumes that J is in the range $J/k_B \sim 1 - 10$ K [53] and that the gyromagnetic ratio is $g = 2$. For Gd-based SOD60, however, a very weak $J/k_B \approx 0.15$ K was estimated [14], which translates into a plateau width of 0.1 T. We note that in the experiments of Ref. [17], the $3/5$ plateau of the Cu-based compound seems to span at least 8 T.

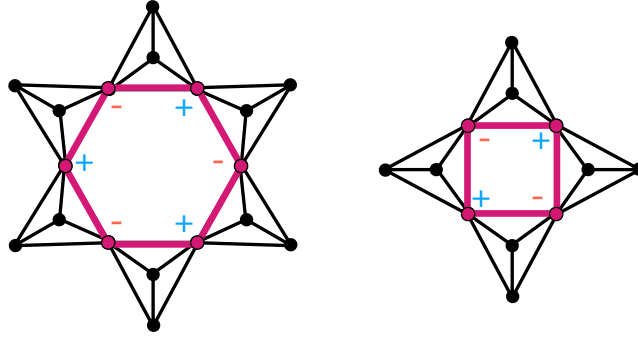


Figure 5: The possible magnon localization domains of the SOD60 molecule on the hexagons and squares (see Sec. 6.1). The \pm sign indicates the amplitude in Eq. (7).

262 saturation ($S_{\text{tot}} = L/2 - 1 = 29$, $M = S_{\text{tot}}$) can be analytically expressed as:

$$|\Psi_{\text{LD}}\rangle = \sum_{l(i) \in \text{LD}} (-1)^{l(i)} S_{l(i)}^- |\uparrow \uparrow \dots \uparrow\rangle, \quad (7)$$

263 where $S_i^- = S_i^x - iS_i^y$ is the spinflip-down operator and LD denotes the bipartite “lo-
 264 calization domain” of the magnon. In our case, the LD is a circular unfrustrated path
 265 of sites, consecutively numbered $l = 0, 1, 2, \dots$, which is sketched in Fig. 5. The proof
 266 that the above expression is an eigenstate is a matter of standard quantum mechanics.
 267 Proving that it is also the lowest-energy state in the sector with $S_{\text{tot}} = L/2 - 1$ is more
 268 difficult [54], but can be readily verified numerically. The localization effect can be un-
 269 derstood in terms of destructive interference: The spinflip terms that would otherwise let
 270 the magnon propagate through the entire lattice cancel exactly if the localized domain is
 271 bounded by triangles. The magnon is thus forced to “run in a circle” on the LD sites with
 272 a momentum of $k = \pi$.

273 For SOD60, we have 14 localized domains given by the 6 squares and the 8 hexagon
 274 faces (see Fig. 5). The change in energy from the fully polarized state (with $E = 144/4 =$
 275 36) due to the presence of one magnon is $\Delta E = 4$. We can continue to add up to $N_{\downarrow} = 6$
 276 magnons that remain noninteracting on spatially separated squares and hexagons. The
 277 ground state energy for fixed $S_{\text{tot}} = L/2 - n$, $n = 0, 1, \dots, 6$, is thus of the linear form
 278 $E = (36 - 4n)$. The corresponding ground state degeneracies are presented in Tab. 3.
 279 They are related to the number of linearly independent ways to arrange the magnons
 280 on the localization domains of the system. The values are thus not obvious, but can be
 281 determined using exact diagonalization.

282 In the regime $S_{\text{tot}} = L/2 - n$, $n = 0, 1, \dots, 6$ the ground-state energy in the presence of
 283 a magnetic field, $E_M(B) = 36 - 4(30 - M) - B \cdot M$, forms a family of curves for different
 284 magnetizations $M := S_{\text{tot}}$ that all intersect at the saturation field of $B_{\text{sat}} = 4$. Above
 285 (slightly below) the saturation field, the fully polarized state with $M = L/2 = 30$ (the
 286 state with $M = L/2 - 6 = 24$) is the ground state. The states with values of M in between
 287 are never the ground state. We thus have a magnetization jump from $M = M_{\text{sat}} = 30$ to
 288 $M = 24 = 4/5 \cdot M_{\text{sat}}$. This is can be seen in Fig. 6.

289 At $B_{\text{sat}} = 4$, all the subspaces become degenerate, and the total degeneracy of the
 290 ground state is given by the sum of all magnon subspaces, $N_{\text{deg}} = 181$. Hence we obtain
 291 a zero-point entropy of $S = \ln(181) k_B \approx 5.2 k_B$ per molecule (or $0.087 k_B$ per spin). For
 292 comparison, on the icosidodecahedron, $S = \ln(38) k_B \approx 3.64 k_B$ per molecule (or $0.121 k_B$
 293 per spin) can be achieved. When the field is varied close to the saturation, the large change
 294 in entropy results in an enhanced magnetocaloric effect [58].

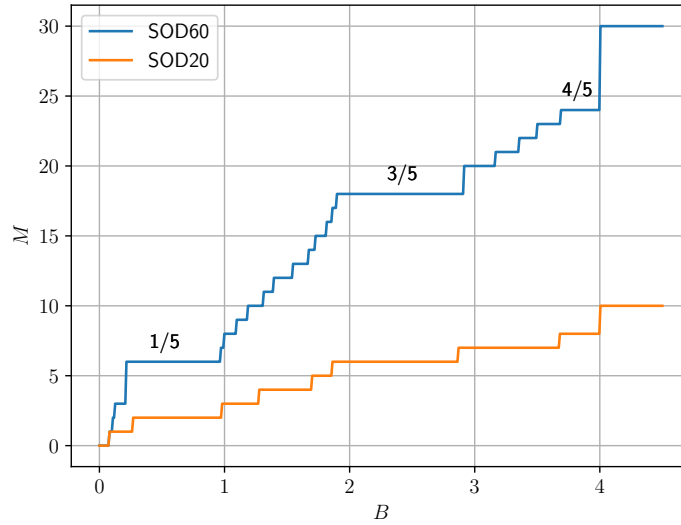


Figure 6: Magnetization $M = \sum_i \langle S_i^z \rangle$ as a function of the applied magnetic field B in the ground state of the SOD60 as well as of the SOD20 molecule.

S_{tot}	$E_0(S_{\text{tot}})$	N_{deg}	N_{magnon}
30	36	1	-
29	32	13	1
28	28	55	2
27	24	71	3
26	20	25	4
25	16	16	5
24	12	1	6
23	8.31(6)	1	-

Table 3: Values of the lowest energy for total spin values close to full saturation ($S_{\text{tot}} = 30$), as well as the corresponding degeneracies. For $S_{\text{tot}} = 29$, there are 13 linearly independent ways to place one localized magnon on the 6 squares and 8 hexagons. For each downstep of S_{tot} , the number of magnons increases by one, the energy decreases linearly, while the number of combinations grows rapidly and peaks at “half-filling” or 3 magnons. For $S_{\text{tot}} = 24$, there is just one combination of arranging the 6 magnons by placing them on all the squares. The effect stops at that point, as can be seen from the deviation from the linear behaviour at $S_{\text{tot}} = 23$.

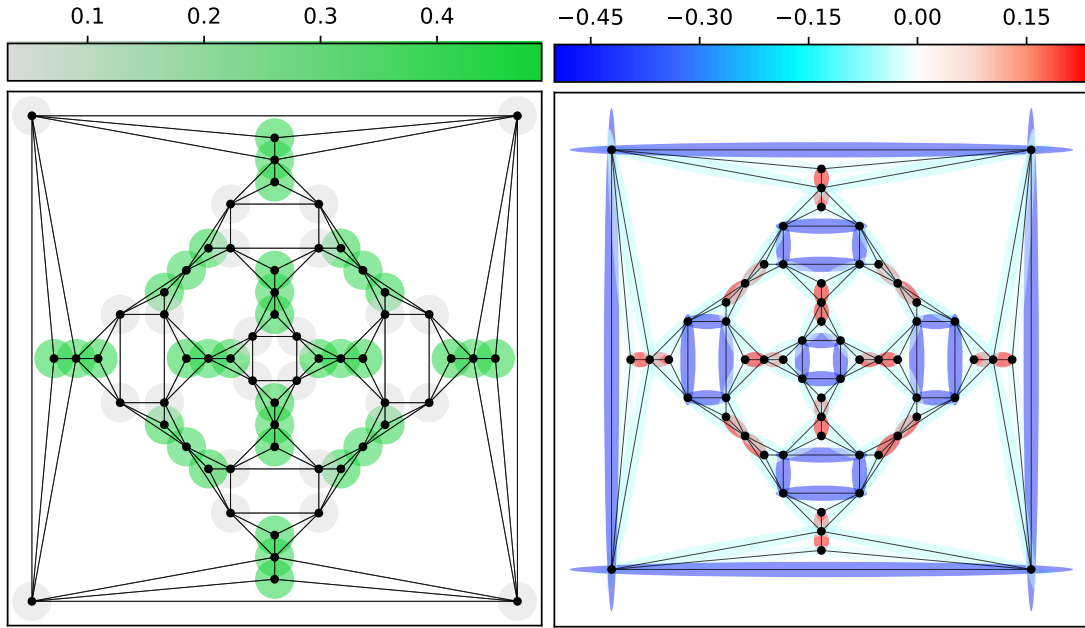


Figure 7: Ground-state properties in the sector $S_{\text{tot}} = 18$ that corresponds to the $3/5$ magnetization plateau. The left and right panel show $\langle \mathbf{S}_i \rangle$ and the nearest-neighbour spin-spin correlations, respectively. Note the appearance of localized singlet states, $\langle \mathbf{S}_i \rangle \approx 0$, with strong antiferromagnetic correlations (the grey sites along the square faces in the left picture).

295 6.2 Localized singlets and doublets

296 The plateaus at $M/M_{\text{sat}} = 3/5$ and $M/M_{\text{sat}} = 1/5$ can be thought of as an extension of the
 297 previous concept from localized magnons to localized singlet clusters: The fraction of $3/5$
 298 corresponds to $N_{\downarrow} = 12$ spinflips, which can be arranged in an antiferromagnetic fashion
 299 on the square faces. Instead of localized one-magnon states, we now have clusters with
 300 $\langle \mathbf{S}_i \rangle \approx 0$ (see Fig. 7). They form a commensurate distribution on the molecule geometry
 301 and optimize the antiferromagnetic exchange energy, thus effectively resisting a change in
 302 magnetization when a field is applied.

303 In contrast, $N_{\downarrow} = 18$ spinflips ($2/5$ configuration) do not lead to an optimal arrange-
 304 ment and do not produce a plateau. For the next magic value of $N_{\downarrow} = 24$ ($1/5$ configu-
 305 ration), the previous distribution of spinflips persists and the additional 12 spinflips can
 306 be arranged on the sites between the hexagons given by 3-site clusters involving two apex
 307 spins (for a 3D impression, cf. the blue bonds in Fig. 3). Their total spin is nearly equal to
 308 $1/2$ and features strong antiferromagnetic correlations (see Fig. 8). This is another stable
 309 configuration that resists a change due to the external field.

310 Overall, we find that the wavefunction at the magic fractions of the saturation is
 311 again characterized by the notion of disconnection. The $4/5$ plateau is governed by 6
 312 independent, localized magnons, which one can show analytically and which is in line
 313 with other frustrated geometries. At the $3/5$ plateau, the localized magnon states become
 314 4-site localized singlet states. Finally, at the $1/5$ plateau, there is additional room for 12
 315 localized spin- $1/2$ states.

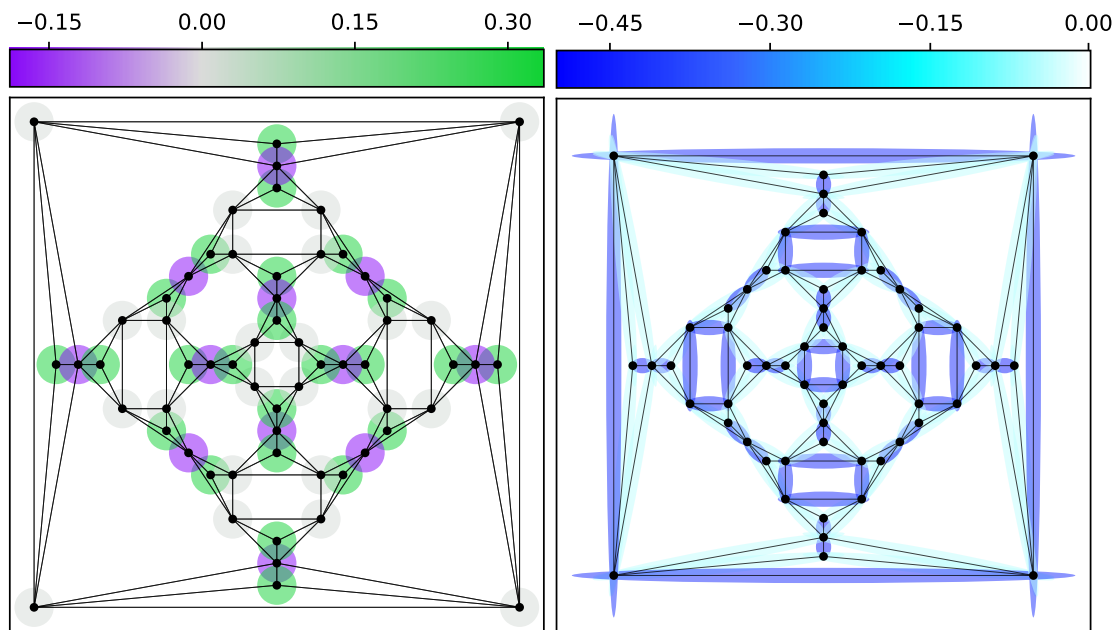


Figure 8: The same as in Fig. 7 but in the sector $S_{\text{tot}} = 6$ that corresponds to the $1/5$ magnetization plateau. Note the additional reduction of the local spin on the 12 sites between the hexagon faces (purple). Correspondingly, the 3-site clusters between the squares now acquire a total spin of $1/2$ and strong antiferromagnetic correlations.

316 7 Conclusion

317 We have analyzed the ground-state properties of the antiferromagnetic $S = 1/2$ Heisenberg
 318 model on the sodalite cage geometry with 24 vertex-sharing tetrahedra using the density
 319 matrix renormalization group. Unlike smaller polyhedra, the ground state is given by
 320 the irreducible representation T and is thus threefold degenerate. One can choose each
 321 member of the ground-state manifold such that it is symmetry-broken and is invariant
 322 only under rotations about one of the three coordinate axes.

323 The spin-spin correlations signal that the molecule breaks up into three large, nearly
 324 disconnected parts. This scenario might be regarded as a generalization of the VBS state,
 325 though the disconnection is not exact. The resulting ground states are difficult to connect
 326 by local updates with a local Hamiltonian. This entails glass-like behaviour within the
 327 DMRG algorithm; standard techniques (such as adding fluctuations) fail, and we need to
 328 apply a global operation by explicitly rotating the state.

329 The physics in the presence of a finite magnetic field is also characterized by confined
 330 clusters which lead to magnetization plateaus at magic fractions of the saturation. We
 331 find localized magnons close to the saturation ($4/5$) that change into nearly-localized 4-
 332 site singlets at the $3/5$ plateau. At the $1/5$ plateau, they are joined by localized 3-site
 333 doublets. These magnetization plateaus are very wide in units of the exchange coupling
 334 J and should thus be observable in the experiment.

335 The results obtained here raise the question whether the ground state for the full
 336 3D pyrochlore lattice may also be crystallized in real space, i.e., breaks the translational
 337 symmetry in some nontrivial way. As discussed in the introduction, results that show
 338 translational symmetry breaking with four sublattices have indeed been obtained in the
 339 past [23, 24, 26]. Thus, it seems plausible that such behaviour is at least a strong tendency
 340 for geometries with vertex-sharing tetrahedra and may appear in various systems of this

341 kind.

342 Apart from the connection to the pyrochlores, the results obtained here outline what
343 can be expected from a spin-liquid system on the sodalite cage geometry in the extreme
344 quantum limit with $S = 1/2$, in particular regarding potential future experiments.

345 Acknowledgements

346 R.R. and C.K. acknowledge support by the Deutsche Forschungsgemeinschaft (DFG, Ger-
347 man Research Foundation) through the Emmy Noether program (KA3360/2-1) as well as
348 by ‘Niedersächsisches Vorab’ through the ‘Quantum- and Nano-Metrology (QUANOMET)’
349 initiative within the project P-1.

350 M.P. is funded by the Deutsche Forschungsgemeinschaft (DFG, German Research
351 Foundation) – 497779765.

352 C.P. is supported by the Deutsche Forschungsgemeinschaft (DFG) through the Cluster
353 of Excellence Advanced Imaging of Matter – EXC 2056 – project ID 390715994.

354 A Symmetry transformations for the SOD60 molecule

355 In order to apply certain symmetry transformations, one has to construct an operator
356 that permutes the sites of the molecule. We are interested in 90° rotations about the
357 three 4-fold symmetry axes connecting the centres of opposite squares. With respect to
358 the Schlegel projection (see Fig. 1), we define a horizontal (h) axis connecting the left and
359 right square, a vertical (v) axis connecting the lower and upper square, and a perpendicular
360 (p) axis connecting the innermost and outermost square. The corresponding permutations
361 of the index set $\{0, \dots, 59\}$ are listed in Tab. 4. All three permutations decompose into
362 15 independent cycles, each consisting of three transpositions.

h	v	p
0 → 17	0 → 30	0 → 12
1 → 31	1 → 29	1 → 10
2 → 16	2 → 44	2 → 24
3 → 25	3 → 15	3 → 4
4 → 32	4 → 18	4 → 11
5 → 6	5 → 45	5 → 25
6 → 18	6 → 46	6 → 26
7 → 24	7 → 13	7 → 1
8 → 12	8 → 14	8 → 0
9 → 26	9 → 5	9 → 3
10 → 47	10 → 16	10 → 22
11 → 40	11 → 6	11 → 9
12 → 48	12 → 17	12 → 23
13 → 2	13 → 53	13 → 31
14 → 0	14 → 43	14 → 17
15 → 5	15 → 54	15 → 32
16 → 29	16 → 55	16 → 39
17 → 30	17 → 48	17 → 41
18 → 15	18 → 56	18 → 40
19 → 10	19 → 27	19 → 2
20 → 4	20 → 28	20 → 6
21 → 11	21 → 20	21 → 5
22 → 39	22 → 2	22 → 7
23 → 41	23 → 0	23 → 8
24 → 55	24 → 31	24 → 36
25 → 46	25 → 32	25 → 38
26 → 56	26 → 25	26 → 37
27 → 1	27 → 42	27 → 16
28 → 3	28 → 35	28 → 18
29 → 13	29 → 59	29 → 47
30 → 14	30 → 58	30 → 48
31 → 44	31 → 47	31 → 51
32 → 45	32 → 40	32 → 52
33 → 22	33 → 19	33 → 13
34 → 23	34 → 8	34 → 14
35 → 9	35 → 21	35 → 15
36 → 51	36 → 1	36 → 19
37 → 38	37 → 3	37 → 20
38 → 52	38 → 4	38 → 21
39 → 59	39 → 24	39 → 49
40 → 54	40 → 26	40 → 50
41 → 58	41 → 12	41 → 34
42 → 7	42 → 33	42 → 29
43 → 8	43 → 34	43 → 30
44 → 27	44 → 57	44 → 55
45 → 20	45 → 50	45 → 46
46 → 28	46 → 52	46 → 56
47 → 53	47 → 39	47 → 57
48 → 43	48 → 41	48 → 58
49 → 36	49 → 7	49 → 27
50 → 37	50 → 9	50 → 28
51 → 57	51 → 10	51 → 33
52 → 50	52 → 11	52 → 35
53 → 19	53 → 49	53 → 44
54 → 21	54 → 37	54 → 45
55 → 42	55 → 51	55 → 59
56 → 35	56 → 38	56 → 54
57 → 49	57 → 22	57 → 42
58 → 34	58 → 23	58 → 43
59 → 33	59 → 36	59 → 53

Table 4: Permutations for the site indices that represent 90° rotations about the specified axes.

References

- 363
- 364 [1] A. Baniodeh, N. Magnani, Y. Lan, G. Buth, C. E. Anson, J. Richter, M. Affronte,
365 J. Schnack and A. K. Powell, *High spin cycles: topping the spin record for a single*
366 *molecule verging on quantum criticality*, npj Quantum Materials **3**(1), 1 (2018).
- 367 [2] J. Schnack, *Large magnetic molecules and what we learn from them*, Contemporary
368 Physics **60**(2), 127 (2019), doi:10.1080/00107514.2019.1615716, [https://doi.org/](https://doi.org/10.1080/00107514.2019.1615716)
369 [10.1080/00107514.2019.1615716](https://doi.org/10.1080/00107514.2019.1615716).
- 370 [3] M. Exler and J. Schnack, *Evaluation of the low-lying energy spectrum of magnetic*
371 *Keplerate molecules using the density-matrix renormalization group technique*, Phys.
372 Rev. B **67**, 094440 (2003), doi:10.1103/PhysRevB.67.094440.
- 373 [4] N. P. Konstantinidis, *Antiferromagnetic Heisenberg model on clusters with icosahedral*
374 *symmetry*, Phys. Rev. B **72**, 064453 (2005), doi:10.1103/PhysRevB.72.064453.
- 375 [5] I. Rousochatzakis, A. M. Läuchli and F. Mila, *Highly frustrated magnetic*
376 *clusters: The kagomé on a sphere*, Phys. Rev. B **77**, 094420 (2008),
377 doi:10.1103/PhysRevB.77.094420.
- 378 [6] J. Schnack and O. Wendland, *Properties of highly frustrated magnetic molecules*
379 *studied by the finite-temperature Lanczos method*, The European Physical Journal B
380 **78**(4), 535 (2010), doi:10.1140/epjb/e2010-10713-8.
- 381 [7] J. Ummethum, J. Schnack and A. M. Läuchli, *Large-scale numerical investigations of*
382 *the antiferromagnetic Heisenberg icosidodecahedron*, Journal of Magnetism and Mag-
383 netic Materials **327**, 103 (2013), doi:<https://doi.org/10.1016/j.jmmm.2012.09.037>.
- 384 [8] N. Kunisada and Y. Fukumoto, *Theoretical study of spherical kagomé clusters in*
385 *Mo72 V30 and W72 V30*, Progress of Theoretical and Experimental Physics **2014**(4)
386 (2014), doi:10.1093/ptep/ptu036, 041I01.
- 387 [9] N. Kunisada and Y. Fukumoto, *Dimer-dimer correlations and magnetothermodynam-*
388 *ics of $S=1/2$ spherical kagome clusters in $W_{72}V_{30}$ and $Mo_{72}V_{30}$* , Physics Procedia
389 **75**, 687 (2015), doi:10.1016/j.phpro.2015.12.089, 20th International Conference on
390 Magnetism, ICM 2015.
- 391 [10] R. Rausch, C. Plorin and M. Peschke, *The antiferromagnetic $S = 1/2$*
392 *Heisenberg model on the C_{60} fullerene geometry*, SciPost Phys. **10**, 87 (2021),
393 doi:10.21468/SciPostPhys.10.4.087.
- 394 [11] A. Müller, A. M. Todea, J. van Slageren, M. Dressel, H. Bögge, M. Schmidtman,
395 M. Luban, L. Engelhardt and M. Rusu, *Triangular geometrical and magnetic motifs*
396 *uniquely linked on a spherical capsule surface*, Angewandte Chemie International
397 Edition **44**(25), 3857 (2005), doi:10.1002/anie.200500697.
- 398 [12] A. M. Todea, A. Merca, H. Bögge, J. van Slageren, M. Dressel, L. Engelhardt,
399 M. Luban, T. Glaser, M. Henry and A. Müller, *Extending the $\{(Mo)Mo_5\}_{12}M_{30}$*
400 *capsule keplerate sequence: A $\{Cr_{30}\}$ cluster of $S=3/2$ metal centers with a*
401 *$\{Na(H_2O)_{12}\}$ encapsulate*, Angewandte Chemie International Edition **46**(32), 6106
402 (2007), doi:10.1002/anie.200700795.

- 403 [13] A. Müller, S. Sarkar, S. Q. N. Shah, H. Bögge, M. Schmidtman, S. Sarkar,
404 P. Kögerler, B. Hauptfleisch, A. X. Trautwein and V. Schünemann, *Archimedean syn-*
405 *thesis and magic numbers: “sizing” giant molybdenum-oxide-based molecular spheres*
406 *of the Keplerate type*, *Angewandte Chemie International Edition* **38**(21), 3238 (1999),
407 doi:10.1002/(SICI)1521-3773(19991102)38:21<3238::AID-ANIE3238>3.0.CO;2-6.
- 408 [14] L. Qin, G.-J. Zhou, Y.-Z. Yu, H. Nojiri, C. Schröder, R. E. P. Winpenny and Y.-Z.
409 Zheng, *Topological self-assembly of highly symmetric lanthanide clusters: A magnetic*
410 *study of exchange-coupling “fingerprints” in giant gadolinium(III) cages*, *Journal of*
411 *the American Chemical Society* **139**(45), 16405 (2017), doi:10.1021/jacs.7b09996,
412 PMID: 29037028, <https://doi.org/10.1021/jacs.7b09996>.
- 413 [15] L. M. Volkova and D. V. Marinin, *Antiferromagnetic spin-frustrated layers*
414 *of corner-sharing Cu₄ tetrahedra on the kagome lattice in volcanic minerals*
415 *Cu₅O₂(VO₄)₂(CuCl), NaCu₅O₂(SeO₃)₂Cl₃, and K₂Cu₅Cl₈(OH)₄·2H₂O*, *Journal of*
416 *Physics: Condensed Matter* **30**(42), 425801 (2018), doi:10.1088/1361-648x/aade0b.
- 417 [16] M. J. Winiarski, T. T. Tran, J. R. Chamorro and T. M. McQueen, *(Cs X)*
418 *Cu₅O₂(PO₄)₂ (X= Cl, Br, I): A family of Cu²⁺ S= 1/2 compounds with capped-*
419 *kagome networks composed of OCu₄ units*, *Inorganic chemistry* **58**(7), 4328 (2019),
420 doi:<https://doi.org/10.1021/acs.inorgchem.8b03464>.
- 421 [17] W. Zhang, Z. He, Y. Xie, M. Cui, S. Zhang, S. Chen, Z. Zhao, M. Zhang and X. Huang,
422 *Molybdate–tellurite compounds with capped-kagome spin–lattices*, *Inorganic chemistry*
423 **59**(4), 2299 (2020), doi:<https://doi.org/10.1021/acs.inorgchem.9b03050>.
- 424 [18] Y. Iqbal, T. Müller, P. Ghosh, M. J. P. Gingras, H. O. Jeschke, S. Rachel,
425 J. Reuther and R. Thomale, *Quantum and classical phases of the pyrochlore*
426 *Heisenberg model with competing interactions*, *Phys. Rev. X* **9**, 011005 (2019),
427 doi:10.1103/PhysRevX.9.011005.
- 428 [19] R. Schäfer, I. Hagymási, R. Moessner and D. J. Luitz, *Pyrochlore $s = \frac{1}{2}$ Heisen-*
429 *berg antiferromagnet at finite temperature*, *Phys. Rev. B* **102**, 054408 (2020),
430 doi:10.1103/PhysRevB.102.054408.
- 431 [20] B. Canals and C. Lacroix, *Pyrochlore antiferromagnet: A three-dimensional quantum*
432 *spin liquid*, *Phys. Rev. Lett.* **80**, 2933 (1998), doi:10.1103/PhysRevLett.80.2933.
- 433 [21] V. R. Chandra and J. Sahoo, *Spin- $\frac{1}{2}$ Heisenberg antiferromagnet on the py-*
434 *rochlore lattice: An exact diagonalization study*, *Phys. Rev. B* **97**, 144407 (2018),
435 doi:10.1103/PhysRevB.97.144407.
- 436 [22] M. Isoda and S. Mori, *Valence-bond crystal and anisotropic excitation spectrum on 3-*
437 *dimensionally frustrated pyrochlore*, *Journal of the Physical Society of Japan* **67**(12),
438 4022 (1998), doi:10.1143/JPSJ.67.4022, <https://doi.org/10.1143/JPSJ.67.4022>.
- 439 [23] A. B. Harris, A. J. Berlinsky and C. Bruder, *Ordering by quantum fluctuations in*
440 *a strongly frustrated Heisenberg antiferromagnet*, *Journal of applied physics* **69**(8),
441 5200 (1991).
- 442 [24] H. Tsunetsugu, *Antiferromagnetic quantum spins on the pyrochlore lattice*, *Journal*
443 *of the Physical Society of Japan* **70**(3), 640 (2001), doi:10.1143/JPSJ.70.640, <https://doi.org/10.1143/JPSJ.70.640>.

- 445 [25] E. Berg, E. Altman and A. Auerbach, *Singlet excitations in pyrochlore:*
446 *A study of quantum frustration*, Phys. Rev. Lett. **90**, 147204 (2003),
447 doi:10.1103/PhysRevLett.90.147204.
- 448 [26] H. Tsunetsugu, *Theory of antiferromagnetic Heisenberg spins on a breathing py-*
449 *rochlore lattice*, Progress of Theoretical and Experimental Physics **2017**(3) (2017),
450 doi:10.1093/ptep/ptx023, 033I01, [https://academic.oup.com/ptep/article-pdf/](https://academic.oup.com/ptep/article-pdf/2017/3/033I01/11136740/ptx023.pdf)
451 [2017/3/033I01/11136740/ptx023.pdf](https://academic.oup.com/ptep/article-pdf/2017/3/033I01/11136740/ptx023.pdf).
- 452 [27] X.-J. Kong, Y. Wu, L.-S. Long, L.-S. Zheng and Z. Zheng, *A chiral 60-metal sodalite*
453 *cage featuring 24 vertex-sharing $[Er_4(\mu_3-OH)_4]$ cubanes*, Journal of the American
454 Chemical Society **131**(20), 6918 (2009), doi:10.1021/ja901214d, [https://doi.org/](https://doi.org/10.1021/ja901214d)
455 [10.1021/ja901214d](https://doi.org/10.1021/ja901214d).
- 456 [28] Y. Wang, T. Han, Y.-S. Ding, Z. Zheng and Y.-Z. Zheng, *Sodalite-like rare-earth car-*
457 *bonates: a study of structural transformation and diluted magnetism*, Dalton Trans.
458 **45**, 1103 (2016), doi:10.1039/C5DT03314D.
- 459 [29] S. J. Miyake, *Spin-wave results for the staggered magnetization of triangular heisen-*
460 *berg antiferromagnet*, Journal of the Physical Society of Japan **61**(3), 983 (1992),
461 doi:10.1143/JPSJ.61.983, <https://doi.org/10.1143/JPSJ.61.983>.
- 462 [30] B. Bernu, P. Lecheminant, C. Lhuillier and L. Pierre, *Exact spectra, spin suscep-*
463 *tibilities, and order parameter of the quantum Heisenberg antiferromagnet on the*
464 *triangular lattice*, Phys. Rev. B **50**, 10048 (1994), doi:10.1103/PhysRevB.50.10048.
- 465 [31] A. V. Chubukov, S. Sachdev and T. Senthil, *Large- s expansion for quantum antiferro-*
466 *magnets on a triangular lattice* **6**(42), 8891 (1994), doi:10.1088/0953-8984/6/42/019.
- 467 [32] L. Capriotti, A. E. Trumper and S. Sorella, *Long-range Néel order*
468 *in the triangular Heisenberg model*, Phys. Rev. Lett. **82**, 3899 (1999),
469 doi:10.1103/PhysRevLett.82.3899.
- 470 [33] C. K. Majumdar and D. K. Ghosh, *On next-nearest-neighbor interaction in linear*
471 *chain. i*, Journal of Mathematical Physics **10**(8), 1388 (1969), doi:10.1063/1.1664978.
- 472 [34] C. K. Majumdar and D. K. Ghosh, *On next-nearest-neighbor interaction in linear*
473 *chain. ii*, Journal of Mathematical Physics **10**(8), 1399 (1969), doi:10.1063/1.1664979.
- 474 [35] B. S. Shastry and B. Sutherland, *Exact ground state of a quantum mechanical anti-*
475 *ferromagnet*, Physica B+ C **108**(1-3), 1069 (1981).
- 476 [36] D. J. Klein, *Exact ground states for a class of antiferromagnetic Heisenberg models*
477 *with short-range interactions*, Journal of Physics A: Mathematical and General **15**(2),
478 661 (1982), doi:10.1088/0305-4470/15/2/032.
- 479 [37] M. E. Fisher, *Statistical mechanics of dimers on a plane lattice*, Phys. Rev. **124**,
480 1664 (1961), doi:10.1103/PhysRev.124.1664.
- 481 [38] D. I. McCooley, *Visual polyhedra*, <http://dmccooley.com/polyhedra/> (2015).
- 482 [39] J. M. Newsam, *The zeolite cage structure*, Science **231**(4742), 1093 (1986),
483 doi:10.1126/science.231.4742.1093, [https://science.sciencemag.org/content/](https://science.sciencemag.org/content/231/4742/1093.full.pdf)
484 [231/4742/1093.full.pdf](https://science.sciencemag.org/content/231/4742/1093.full.pdf).

- 485 [40] Q.-F. Sun, S. Sato and M. Fujita, *An m_18l_24 stellated cuboctahedron through post-*
486 *stellation of an m_12l_24 core*, Nature chemistry **4**(4), 330 (2012).
- 487 [41] S. Kang, H. Zheng, T. Liu, K. Hamachi, S. Kanegawa, K. Sugimoto, Y. Shiota,
488 S. Hayami, M. Mito, T. Nakamura *et al.*, *A ferromagnetically coupled fe_2 cyanide-*
489 *bridged nanocage*, Nature communications **6**(1), 1 (2015).
- 490 [42] U. Schollwöck, *The density-matrix renormalization group in the*
491 *age of matrix product states*, Annals of Physics **326**, 96 (2011),
492 doi:<https://doi.org/10.1016/j.aop.2010.09.012>.
- 493 [43] I. P. McCulloch, *From density-matrix renormalization group to matrix product states*,
494 Journal of Statistical Mechanics: Theory and Experiment **2007**(10), P10014 (2007),
495 doi:10.1088/1742-5468/2007/10/p10014.
- 496 [44] E. Cuthill and J. McKee, *Reducing the bandwidth of sparse symmetric matrices*,
497 In *Proceedings of the 1969 24th National Conference*, ACM '69, p. 157–172. As-
498 sociation for Computing Machinery, New York, NY, USA, ISBN 9781450374934,
499 doi:10.1145/800195.805928 (1969).
- 500 [45] C. Hubig, I. P. McCulloch and U. Schollwöck, *Generic construction of efficient matrix*
501 *product operators*, Phys. Rev. B **95**, 035129 (2017), doi:10.1103/PhysRevB.95.035129.
- 502 [46] P. A. M. Dirac, *Quantum mechanics of many-electron systems*, Proceedings of the
503 Royal Society of London. Series A, Containing Papers of a Mathematical and Physical
504 Character **123**(792), 714 (1929).
- 505 [47] H. Diep *et al.*, *Frustrated spin systems*, World Scientific (2013).
- 506 [48] C. Lacroix, P. Mendels and F. Mila, *Introduction to frustrated magnetism: materials,*
507 *experiments, theory*, vol. 164, Springer Science & Business Media (2011).
- 508 [49] E. Fradkin, *Field theories of condensed matter physics*, Cambridge University Press
509 (2013).
- 510 [50] L. Savary and L. Balents, *Quantum spin liquids: a review*, Reports on Progress in
511 Physics **80**(1), 016502 (2016), doi:10.1088/0034-4885/80/1/016502.
- 512 [51] M. Kohmoto and B. Sutherland, *Electronic and vibrational modes on a Pen-*
513 *rose lattice: Localized states and band structure*, Phys. Rev. B **34**, 3849 (1986),
514 doi:10.1103/PhysRevB.34.3849.
- 515 [52] M. Arai, T. Tokihiro, T. Fujiwara and M. Kohmoto, *Strictly localized*
516 *states on a two-dimensional Penrose lattice*, Phys. Rev. B **38**, 1621 (1988),
517 doi:10.1103/PhysRevB.38.1621.
- 518 [53] L. Peters, S. Ghosh, B. Sanyal, C. van Dijk, J. Bowlan, W. de Heer, A. Delin,
519 I. Di Marco, O. Eriksson, M. I. Katsnelson *et al.*, *Magnetism and exchange in-*
520 *teraction of small rare-earth clusters; Tb as a representative*, Scientific reports **6**(1),
521 1 (2016).
- 522 [54] J. Schnack, H.-J. Schmidt, J. Richter and J. Schulenburg, *Independent magnon states*
523 *on magnetic polytopes*, The European Physical Journal B-Condensed Matter and
524 Complex Systems **24**(4), 475 (2001).

- 525 [55] J. Schulenburg, A. Honecker, J. Schnack, J. Richter and H.-J. Schmidt, *Macroscopic*
526 *magnetization jumps due to independent magnons in frustrated quantum spin lattices*,
527 *Phys. Rev. Lett.* **88**, 167207 (2002), doi:10.1103/PhysRevLett.88.167207.
- 528 [56] J. Richter, J. Schulenburg, A. Honecker, J. Schnack and H.-J. Schmidt, *Exact*
529 *eigenstates and macroscopic magnetization jumps in strongly frustrated spin lat-*
530 *tices*, *Journal of Physics: Condensed Matter* **16**(11), S779 (2004), doi:10.1088/0953-
531 8984/16/11/029.
- 532 [57] J. Richter, *Localized-magnon states in strongly frustrated quantum spin lattices*, *Low*
533 *Temperature Physics* **31**(8), 695 (2005).
- 534 [58] J. Schnack, R. Schmidt and J. Richter, *Enhanced magnetocaloric effect in frustrated*
535 *magnetic molecules with icosahedral symmetry*, *Phys. Rev. B* **76**, 054413 (2007),
536 doi:10.1103/PhysRevB.76.054413.
- 537 [59] J. Schnack, J. Schulenburg, A. Honecker and J. Richter, *Magnon crystalliza-*
538 *tion in the kagome lattice antiferromagnet*, *Phys. Rev. Lett.* **125**, 117207 (2020),
539 doi:10.1103/PhysRevLett.125.117207.